Ultrasonic Multi-Hole Imaging Using Full Waveform Inversion

SHOAIB ANWAR, MD. AKTHARUZZAMAN, JOHN DAY and JIAZE HE

ABSTRACT

Ultrasound computed tomography (USCT), in recent years, is becoming an increasingly popular method for structural health monitoring (SHM) and non-destructive evaluation (NDE). Full waveform inversion (FWI), a cutting-edge inversion method, utilizes all information in ultrasonic measurements in USCT. It iteratively reconstructs the model parameters (i.e., wave speed of materials) of the scanned specimen by calculating the gradient of waveform difference between the measured and synthetic signals through a partial derivative equation (PDE)-constrained optimization process. By reconstructing these model parameters, defects inside the specimen can be identified. This study aims to evaluate FWI's performance in imaging defects (i.e., holes). FWI was implemented to process the numerically generated signals to simulate the data acquisition in a steel specimen with six holes of different sizes (diameters ranging from 0.4 mm to 5.2 mm). First, a shorter numerical model with the same number and size of holes was used to benchmark FWI's performance with full coverage of source and receiver elements for the domain. To emulate large-scale structural component inspection, the numerical domain was then changed to the dimensions of the actual steel specimen, and the scanning setup was changed to a pair of linear transducer arrays with relatively shorter apertures located on the top and bottom of the specimen. The effect of the array aperture on the FWI performance was studied. The reconstructed model parameter, longitudinal wave speed (V_p) , and shear wave speed (V_s) maps showed that with the current setup, FWI can identify the locations of all holes. A new imaging condition was proposed using the inverted V_p and V_s maps to quantify the shapes and size of the holes. The ultrasound signals from the actual steel specimen with holes of the same dimensions were also analyzed and modeled. The results exhibit the potential of applying FWI on experimentally acquired data from the steel sample.

Shoaib Anwar, Aerospace Engineering and Mechanics, The University of Alabama, Tuscaloosa, AL, USA
Md. Akhtaruzzaman, Aerospace Engineering and Mechanics, The University of Alabama, Tuscaloosa, AL, USA
John Day, Aerospace Engineering and Mechanics, The University of Alabama, Tuscaloosa, AL, USA. Jiaze He, Aerospace Engineering and Mechanics, The University of Alabama, Tuscaloosa, AL, USA
*Corresponding author, Email: jhe26@eng.ua.edu

INTRODUCTION

In recent years, inversion-based diagnostics using ultrasound computed tomography (USCT) have gained much attention. Methods such as a straight-ray tomographic reconstruction (Lamb-wave or guided-wave tomography) [1] and total focusing method (TFM) [2] have gained success in reconstructing complex geometry like composite material and additive material (AM). However, such methods do not utilize all information about ultrasound signals. Hence, detailed wave propagation physics is not properly addressed. To resolve wave modeling, various numerical approaches can be adopted. Full waveform inversion (FWI) is one of the inversion techniques to invert the parameters (such as wave speed, density, and attenuation) which are directly related to material properties [3]. In such an approach, the misfit between the obtained wave signals and the synthetic data generated through numerical modeling is minimized by calculating the gradient for the model parameters iteratively. This optimization technique allows the number of computations independent from the number of parameters and avoids directly solving excessively complex global optimization for imaging. This method uses the complete information of the ultrasound signals and is thus able to reconstruct the model with high resolution.

Being immensely popular in geophysics studies for global tomography, FWI is also being adopted in structural health monitoring (SHM) and non-destructive evaluation (NDE) [4]. However, FWI is still in its infancy in reconstructions for complex structures. Its ability to perform multiparameter inversion and recreate high-resolution models from ultrasound signals have made it favorable for reconstructing complex structures with defects [5–7]. He *et al.* implemented FWI to reconstruct polycrystalline grain distribution [8]. Nguyen *et al.* also used low-frequency FWI with high-frequency RTM for imaging defects in heterogeneous structures [9].

In this paper, the performance of FWI was evaluated using numerical models of a steel sample with holes of various sizes. The aim is to detect the position, shapes, and sizes of the holes in the structure by reconstructing the longitudinal (V_p) and shear (V_s) velocity maps using FWI. The numerical cases were designed to represent a steel specimen with a length and width of the specimen were 154.2 mm and 32 mm, respectively, as shown in Figure 1. It had six drilled holes with diameters of 5.16, 3.175, 1.985, 1.1384, 1.1106, and 0.6984 mm at the horizontal center line. The distances of the hole centers from the left wall (wall near the big hole) were 48.15, 61.83, 74.35, 86.2, 96.55, and 106.75 mm, respectively. FWI was carried out with both surrounding (larger aperture) and transmission scanning configuration (shorter aperture) scanning configuration. While the first scanning setup produced quantitative reconstructions regarding holes' locations, size, and shape, the velocity map reconstruction with the later one was compromised when using limited aperture data acquisition. To alleviate the reconstruction distortion, we have proposed an imaging condition to combine both the V_p and V_s maps to further quantify the hole's positions, size, and shape.

The remainder of the paper is organized as follows. First, the principles of FWI are introduced. Then FWI's performance was benchmarked with a shorter numerical model and an ideal scanning setup. Next, the performance of FWI in the numerical models with dimensions of the actual specimen and more practical scanning setups has been discussed. Finally, the results are summarised in the conclusion.

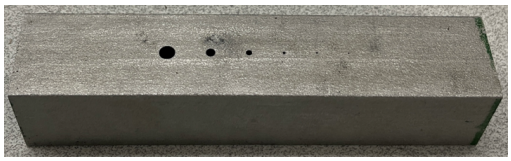

Figure 1. Actual steel sample with a dimension of 154.2 mm $\times$ 32 mm. It has six holes with varying diameters at the center horizontal line. All numerical models were built on this steel sample.

METHODOLOGY: FULL WAVEFORM INVERSION FRAMEWORK

FWI is a non-linear inversion approach that iteratively minimizes the gradient of the misfit function between real and synthetic data to determine model parameters [3, 7]. The first step of the procedure is to choose sources and an approximate model, which is referred to as an initial model. A spectral element method (SEM) is performed with this initial model to create the synthetic data. This process is called forward simulation [7]. In this study, the FEA is done by a 2D spectral element-based solver called SPECFEM2D [10]. Initially, the difference or misfit between the synthetic data and the true model data is expected to be large. To reduce this misfit between these two model data, an adjoint simulation is performed to update the synthetic data. This process entails introducing 'adjoint sources' as source time functions at the location of receivers and back-projecting the measured data difference and finally optimizing the simulated model. The model parameters are determined by the interaction of the forward and adjoint wavefields. This process is repeated until the misfit is less than a preset value (ε), at which point a high-resolution numerical model of the defect/material distribution is reconstructed as the final model. A modified version of SeisFlows, a Python-based framework, to implement FWI in this research [10].

BENCHMARK THE FWI PERFORMANCE

A numerical domain of 80 mm $\times$ 32 mm with six holes (with the same diameter as the actual steel sample) was considered as a benchmarking model. A finite element mesh generator called Gmsh was used to build the model. This model was labeled as the 'True Model'. Density (i.e., ρ), V_p and V_s of the model were 7850.0 ($\mathrm{kg/m^3}$), 5591.8 (m/s) and 3090.9 (m/s), respectively. For our 'Initial Model', a flawless (without any holes) domain with the same dimension was designed. The performance of FWI depends much on the accuracy of material properties of the initial model [5]. As the objective of this study is to reconstruct the image of the holes only, the material properties of the initial guessed model were kept the same as the true model to limit the constraints of FWI performance. Figure 2 (a) and (b) illustrate the unstructured mesh of the initial model and true model, respectively. Furthermore, to avoid complexity the variation in material density and effect of attenuation were neglected [8].

For creating the scanning setup, four linear arrays with multiple source elements near four boundary walls were used to ensure that the results were devoid of the potential for spatial aliasing [7]. The top and bottom arrays consisted of 24 evenly spaced elements each and the side arrays consisted of 8 evenly spaced elements each (Figure 2 (c)). Each element was excited individually to create a narrow-banded Ricker signal of 0.5 MHz

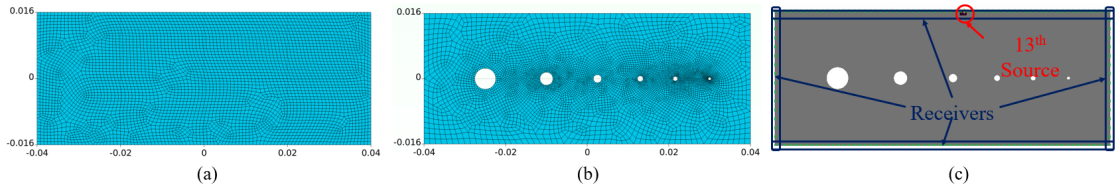

Figure 2. Unstructured mesh of (a) the flawless initial model and (b) the true model with 6 holes of varying sizes for benchmarking the FWI performance. Gmsh was used to generate these mesh. (c) illustrates the position of the source (red circle) and the surrounding receivers (blue boxes).

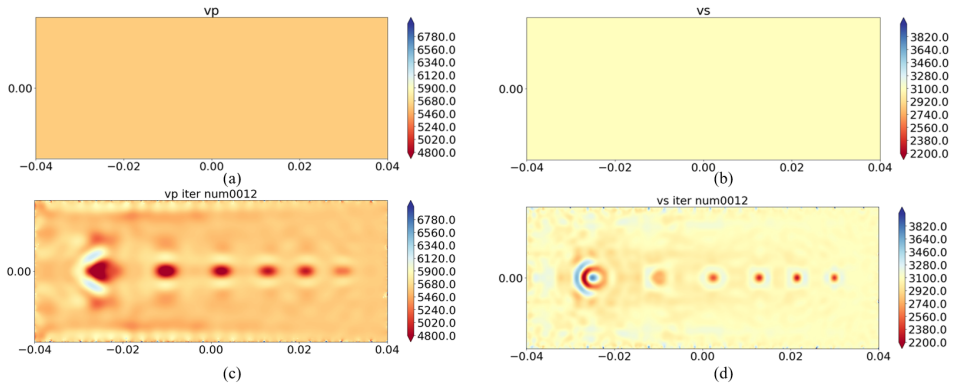

Figure 3. (a) and (b) are the V_p and V_s maps of the initial model, respectively. (c) and (d) are the respective reconstructed velocity maps after the 23rd FWI iteration.

center frequency. Hence, a total of 64 excitation events (forward modeling) were used in the benchmarking process. To catch the signals, a total of 156 sensor elements (receivers) were positioned around the four boundaries.

FWI was performed with this scanning setup and the aim was to reconstruct the V_p and V_s maps from the initial model (Figure 3 (a) and (b)). Hence, detect the hole positions, sizes, and shapes. Throughout the simulation, the center frequency was 0.5 MHz making the V_p and V_s wavelengthes to be 11.184 mm (e.g., more than twice of the largest hole diameter (5.16 mm)) and 6.182 mm, respectively. Consequently, reconstructing the V_p map near larger holes is presumably prone to artifacts [11]. Figure 3 (c) and (d) show the inverted V_p and V_s maps, respectively. Consistent with expectations, with the current setup, FWI struggled to reconstruct the V_p map near the largest hole, resulting in a distorted shape and size of the largest hole. However, the other holes' locations were imaged with slightly overestimated shapes and sizes. In contrast, due to the shorter wavelength in the V_s map, the inverted V_s map was sharper than the V_p map, and the holes' locations, shapes, and sizes were inverted more precisely.

APERTURE EFFECTS OF FWI ON MULTI-HOLE IMAGING

While the surrounding scanning setup with a larger aperture of the benchmarking model was ideal for FWI, it is less practical for scanning a longer domain. Figure 4 (a) and (b) show the initial model and the true model having the same dimensions as the actual steel block (154 mm $\times$ 32 mm). The material properties, as well as the diameters and positions of the holes with respect to the center lines of the domain, were the same

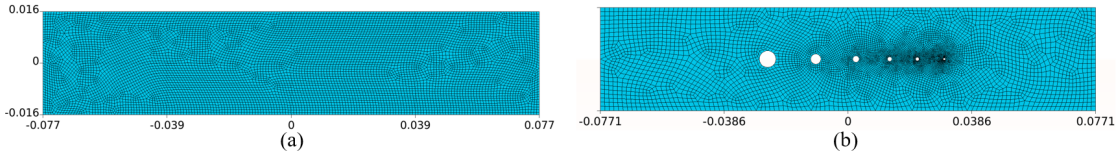

Figure 4. Unstructured mesh of (a) the flawless initial model and (b) the true model with the same dimensions as the actual steel. Gmsh was used to generate these mesh.

as the benchmarking model. Due to the limitations imposed by the experimental setup, placing receivers at the side walls of this longer domain was unfeasible. Furthermore, this posed a challenge, as ultrasonic waves excited from a source at the center of the top wall of the domain would undergo multiple reflections between the bottom and top walls prior to reaching the side walls. Therefore, in the scanning setup, a single array consisting of 32 source elements was placed at the top wall, while 32 receiver elements were located at the opposite bottom wall, thereby facilitating a transmission mode scanning approach. The spatial distribution of both the source and receiver elements was uniform and covered a length of 62 mm within their respective arrays. Similar to the benchmarking model, each source element was excited individually to generate a narrow-banded Ricker signal of 0.5 MHz center frequency. Therefore, 32 excitation events were used in this FWI process. To scan the entire domain, this configuration was applied in three distinct locations. Accordingly, three FWI simulations were conducted, each comprising 32 events. These three simulations are referred to as Case-i, Case-ii, and Case-iii. Figures 5 (a), 6 (a), and 7 (a) illustrate the locations of the scanning configurations of these three cases, respectively. The reconstructed V_p maps demonstrated (Figures 5 (b), 6 (b) and 7 (b) for Case-i, ii, iii, respectively) similar results as the benchmarked model despite of having no side wall receivers' information. In all three cases, the locations and relative sizes of the holes were detected but they suffered from the overestimation of the sizes and shapes. Interestingly, the invited V_p maps show the current FWI setup was able to collect information from the wave reflections from the holes outside of the scanning region (between the dashed lines in Figures 5 (a), and 7 (a)). In particular, the third hole in Case-i and the second hole in Case-iii were detected in the reconstructed velocity maps though they were outside of the scanning region. On the other hand, due to the short aperture and lack of side wall receivers, the information regarding the V_s was not as effective as that of V_p. This justifies the extremely distorted reconstruction of the V_s maps for all three cases (Figures 5 (c), 6 (c) and 7 (c) for Case-i, ii, iii, respectively).

In spite of the distorted shapes and sizes of the holes in both inverted V_p and V_s maps, they exhibited a noticeable pattern. The distortion in the V_p maps occurred in the horizontal direction, while the shapes in the V_s maps were distorted vertically. To address this issue, we have proposed an imaging condition to quantify the shape and size of the holes as follows. At first, both velocity maps were normalized from 0 to 1 and then calculated the statistical mean of the normalized velocities at each point of the domain. To remove the artifacts created by the scattered wave, a mask was used which filtered out the normalized-mean velocity values above 0.5. The resulting mean-velocity maps from the normalized V_p and V_s are presented in Figures 5 (d), 6 (d), and 7 (d) for Cases-i, ii, and iii, respectively. This method not only enabled the accurate identification of the hole locations, shapes, and sizes, particularly for Cases-ii and iii but also facilitated the

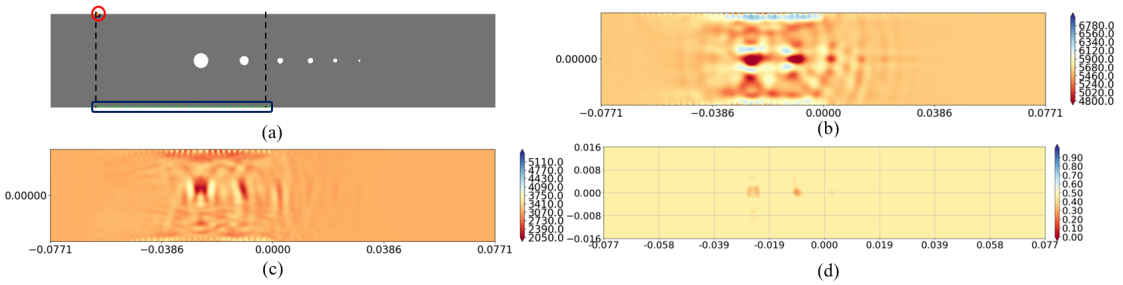

Figure 5. Case-i: (a) Location of the scanning setup. The red circle region is pointing to the location of the source of the 1st excitation event out of 32 events of FWI and the blue box is referring to the position of the 32 receiver elements. Reconstructed (b) V_p and (c) V_s maps. (d) Mean-velocity map derived from the normalized V_p and V_s.

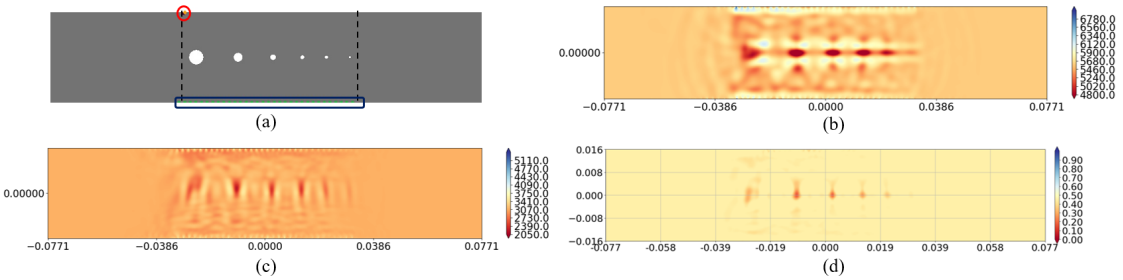

Figure 6. Case-ii: (a) Location of the scanning setup. The red circle region is pointing to the location of the source of the 1st excitation event out of 32 events of FWI and the blue box is referring to the position of the 32 receiver elements. Reconstructed (b) V_p and (c) V_s maps. (d) Mean-velocity map derived from the normalized V_p and V_s.

removal of unwanted artifacts around the holes.

DATA ACQUISITION WITH THE EXPERIMENTAL SETUP

The numerical study has shown promise for implementing the current FWI setup in experimentally acquired data. Figure 8 (a) depicts the experimental scanning setup used for acquiring data from the steel block, similar to Case-ii. To acquire data for the steel sample, a multi-channel data acquisition (DAQ) system from Verasonics was used to capture full matrix-captured (FMC) data. Recently, our group published a paper, which discussed the generation of an inverted source time function (STF) and using it for the material characterization of an aluminum block [12]. Using that inverted STF in Case-ii, a forward modeling simulation with a single source element (15th element of the case) and 32 receiver elements was executed. A comparison of the B-scan signal of the 15th element of this simulation and the B-scan signal at a similar location from the acquired FMC data from the experiment is shown in Figure 8 (b). Both signals aligned closely with some discrepancies. This could be due to the mismatch in the location of the element in the numerical model and the actual transducer position in the experiment with respect to the holes. Furthermore, the effect of outer plane signals in the experiment was ignored while creating the inverted STF which can also be a reason for these differences. Future studies will focus on addressing this issue and imaging with experimentally acquired data with the real steel block.

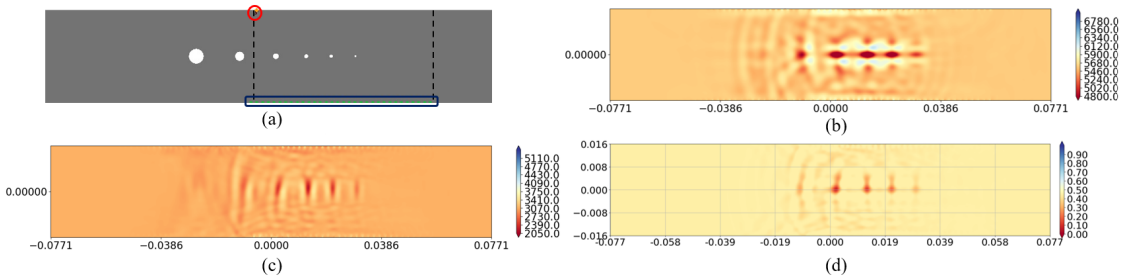

Figure 7. Case-iii: (a) Location of the scanning setup. The red circle region is pointing to the location of the source of the 1st excitation event out of 32 events of FWI and the blue box is referring to the position of the 32 receiver elements. Reconstructed (b) V_p and (c) V_s maps. (d) Mean-velocity map derived from the normalized V_p and V_s.

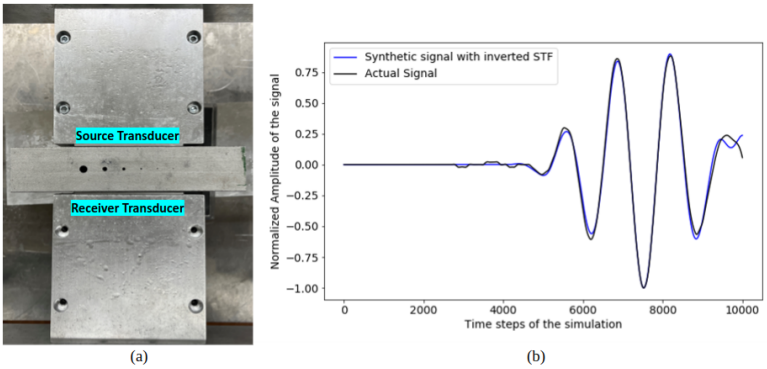

Figure 8. (a) Experimental setup to scan the real steel sample. This setup is analogous to the scanning configuration of Case-ii, where the source and station arrays were located at the center of the top and bottom walls respectively. (b) Comparison of the B-scan synthetic signal of the 15th element of the numerical model (Case-ii) using the inverted STF with the acquired B-scan signal of the 15th element of the experimental signal [12].

CONCLUSION

In this study, FWI was applied to reconstruct the V_p and V_s maps of a multi-hole steel specimen using ultrasound signals. The process was benchmarked with a smaller model that had the same number and diameter of holes, acquiring ultrasound signals from all sides of the domain to create a wide aperture scanning setup. The FWI process successfully reconstructed the V_s map, accurately detecting the locations, sizes, and shapes of the holes. However, the reconstruction of V_p was slightly compromised in detecting the sizes and shapes of the holes.

To simulate large-scale inspection, the scanning configuration was then changed to a pair of linear transducer arrays, creating a shorter aperture without side wall transducer elements. A longer numerical model was designed with the same dimensions as the actual steel specimen in the lab and three FWI simulations were conducted with the numerically generated scanned data at three different locations of the domain. The results showed that the shorter scanning configuration had less effects on inverting V_p maps. However, it significantly impacted the reconstruction of the V_s maps.

To quantify the locations, shapes, and sizes of the holes, we proposed a new strategy to compute the statistical mean of the normalized V_p and V_s of every point of the domain.

This strategy was able to accurately identify the locations, shapes, and sizes of the holes except for the largest one.

Finally, the potential of implementing the current FWI for multi-hole imaging of the steel sample was discussed demonstrating the signals acquired from the actual experiment. Overall, our results suggest that FWI can be a promising method for non-destructive evaluation and structural health monitoring of multi-hole structures.

ACKNOWLEDGMENT

We appreciate the financial support provided by NASA Project #80NSSC22M0223 and the computational resources provided by ACCESS Project #MDE220005.

REFERENCES

1. Leonard, K. R., E. V. Malyarenko, and M. K. Hinders. 2002. "Ultrasonic Lamb wave tomography," *Inverse problems*, 18(6):1795.
2. Chabot, A., N. Laroche, E. Carcreff, M. Rauch, and J.-Y. Hascoët. 2020. "Towards defect monitoring for metallic additive manufacturing components using phased array ultrasonic testing," *Journal of Intelligent Manufacturing*, 31(5):1191–1201.
3. Tromp, J., C. Tape, and Q. Liu. 2005. "Seismic tomography, adjoint methods, time reversal and banana-doughnut kernels," *Geophysical Journal International*, 160(1):195–216.
4. Lamert, A., L. T. Nguyen, W. Friederich, and T. Nestorović. 2018. "Imaging disturbance zones ahead of a tunnel by elastic full-waveform inversion: Adjoint gradient based inversion vs. parameter space reduction using a level-set method," *Underground Space*, 3(1):21–33.
5. Operto, S., Y. Gholami, V. Prieux, A. Ribodetti, R. Brossier, L. Metivier, and J. Virieux. 2013. "A guided tour of multiparameter full-waveform inversion with multicomponent data: From theory to practice," *The leading edge*, 32(9):1040–1054.
6. Sun, M., J. Yang, L. Dong, Y. Liu, and C. Huang. 2017. "Density reconstruction in multiparameter elastic full-waveform inversion," *Journal of Geophysics and Engineering*, 14(6):1445–1462.
7. He, J., J. Rao, J. D. Fleming, H. N. Gharti, L. T. Nguyen, and G. Morrison. 2021. "Numerical ultrasonic full waveform inversion (FWI) for complex structures in coupled 2D solid/fluid media," *Smart Materials and Structures*, 30(8):085044.
8. He, J., D. Borisov, J. D. Fleming, and M. Kasemer. 2022. "Subsurface polycrystalline reconstruction based on full waveform inversion-A 2D numerical study," *Materialia*, 24:101482.
9. Nguyen, L. T. and R. T. Modrak. 2018. "Ultrasonic wavefield inversion and migration in complex heterogeneous structures: 2D numerical imaging and nondestructive testing experiments," *Ultrasonics*, 82:357–370.
10. Modrak, R. T., D. Borisov, M. Lefebvre, and J. Tromp. 2018. "SeisFlows—Flexible waveform inversion software," *Computers & geosciences*, 115:88–95.
11. Virieux, J. and S. Operto. 2009. "An overview of full-waveform inversion in exploration geophysics," *Geophysics*, 74(6):WCC1–WCC26.
12. Aktharuzzaman, M., S. Anwar, D. Borisov, J. Rao, and J. He. 2022. "2D Numerical Ultrasound Computed Tomography for Elastic Material Properties in Metals," in *ASME International Mechanical Engineering Congress and Exposition*, American Society of Mechanical Engineers, vol. 86625, p. V001T01A012.